# Critical gradient formula for toroidal electron temperature gradient modes

F. Jenko, W. Dorland,[a] and G. W. Hammett[b]
*Max-Planck-Institut für Plasmaphysik, EURATOM Association, 85748 Garching, Germany*

(Received 9 March 2001; accepted 18 June 2001)

Under certain conditions, the electron heat transport induced by electron temperature gradient (ETG) streamers is sufficiently large and sensitive with respect to the normalized electron temperature gradient to represent a possible cause for electron temperature profile consistency (''stiffness''). Here, linear gyrokinetic simulations of toroidal ETG modes in tokamak core and edge plasmas are presented. An algebraic formula for the threshold of the linear instability is derived from the numerical solutions of the linear gyrokinetic equations which recovers previous analytical results in the appropriate limits. © *2001 American Institute of Physics.*
[DOI: 10.1063/1.1391261]

## I. INTRODUCTION

Recent nonlinear gyrokinetic simulations have shown that hyperfine-scale turbulence (at perpendicular spatial scales comparable to or smaller than the ion gyroradius) driven by electron temperature gradient (ETG) modes can yield electron heat flux levels which greatly exceed simple mixing length estimates.[1,2] This surprising finding is linked to the presence of radially highly elongated vortices (''streamers'') which lead to very efficient turbulent convection down the gradient. Furthermore, under typical tokamak core conditions one can expect the linear critical temperature gradient and the streamer onset condition to be almost the same.[3] (This is not the case, however, for plasmas with negative shear or steep gradient regions.) ETG streamers may therefore play a role in explaining the ''stiffness'' of $T_e$ profiles that is observed in many experiments. This term is used to describe the fact that $T_e$ profiles sometimes do not react much to a substantial increase in the applied heating power (and corresponding radial heat flux). A sharp increase of the turbulent electron heat flux with increasing normalized $T_e$ gradient as observed in Ref. 3 could be consistent with this experimental observation. Given the possible relevance of the linear threshold of toroidal ETG modes, we perform a large number of linear gyrokinetic simulations to study its dependence on various plasma parameters, and find a compact algebraic formula. We discuss the results with respect to previous analytical results and to experimental observations.

Note that for sufficiently flat density profiles, trapped electron modes (TEMs) also exhibit a linear threshold and are therefore capable of producing $T_e$ profile stiffness.[3] In the presence of *two* critical $T_e$ gradients (from both ETG modes *and* TEMs), the mode with the smaller value of $(R/L_{T_e})_{\mathrm{crit}}$ may be the most interesting. Here, however, we restrict our attention to the linear ETG threshold. The study of the linear TEM threshold will be the subject of another paper.

In the linear, electrostatic, adiabatic limit, ETG modes and ion temperature gradient (ITG) modes are basically isomorphic, i.e., known ITG results can be turned into ETG results (and vice versa) by switching the role of ions and electrons. However, there are a number of effects in which these two modes differ even linearly: (1) nonadiabatic effects (ITG, trapped and passing electron dynamics on similar perpendicular scales; ETG, ion dynamics on larger perpendicular scales), (2) electromagnetic effects (the collisionless skin depth lies between the electron and ion gyroradius for typical tokamak parameters), and (3) Debye shielding effects which can stabilize the ETG mode if the electron Debye length $\lambda_{\mathrm{De}}$ exceeds the electron gyroradius $\rho_e$ (see the corresponding remarks in Ref. 1). Nonadiabatic and electromagnetic effects will be addressed below, whereas Debye shielding effects will be neglected since in general $\lambda_{\mathrm{De}}/\rho_e \approx B_T/n_{e19}^{1/2} \lesssim 1$ (where $B_T$ is the toroidal magnetic field in units of Tesla and $n_{e19}$ is the electron density in units of $10^{19}\,\mathrm{m}^{-3}$). Debye shielding effects therefore play a small role except close to the edge where the density is very low and the profile gradients are very steep so that the linear poloidal wave-number spectrum is shifted to larger values where it is more susceptible to Debye length effects. However, in deriving our critical gradient formula for ETG modes, we will focus on standard core parameters for which the linear ETG threshold is expected to be most relevant.

## II. LINEAR GYROKINETIC SIMULATIONS: CRITICAL GRADIENTS

To investigate the dependence of the critical gradient for toroidal ETG modes on various plasma parameters, we employ a linear gyrokinetic code, GS2.[4] It solves the gyrokinetic Vlasov–Maxwell equations[5,6] and includes both passing and trapped particles, electromagnetic effects, as well as a Lorentz collision operator. Although GS2 is designed to work in general tokamak geometry, we will focus mainly on a large aspect ratio, circular flux surface magnetohydrody-

[a]University of Maryland, College Park, Maryland 20742.
[b]Princeton Plasma Physics Laboratory, Princeton University, P.O. Box 451, Princeton, New Jersey 08543.

 

namic model equilibrium[7] which is characterized by magnetic shear, $\hat{s}$, and the normalized pressure gradient, $\alpha$.

We consider a plasma consisting of electrons and one ion species of charge $Z_i$. Thus, the relevant physical parameters (besides $\hat{s}$ and $\alpha$) are the normalized electron and ion temperature gradients, $R/L_{T_e}$ and $R/L_{T_i}$, the normalized density gradient, $R/L_n$, the electron to ion temperature ratio, $T_e/T_i$, the ion to electron mass ratio, $m_i/m_e$, the total plasma beta, $\beta=8\pi p/B^2$, the safety factor, $q$, and the normalized electron–ion collision frequency, $\nu_{ei}R/v_{te}$. Here, normalized gradients are defined by $R/L_T \equiv -(R/T)(dT/dr)$ where $R$ is the major radius. The quantity $v_{te}$ is the thermal electron velocity, $v_{te}^2=T_e/m_e$. Whenever we vary one of these parameters, it is assumed that we hold the rest of them fixed. This means, e.g., that we will vary $R/L_n$ at constant $R/L_{T_e}$ and not at constant $\eta_e=L_n/L_{T_e}$. For ETG modes at perpendicular spatial scales smaller than the ion gyroradius, the gyrokinetic Poisson's equation yields an adiabatic ion response which leads to $\tilde{n}_e/n_e=-\tau(e\Phi/T_e)$ where $\tau=Z_i(T_e/T_i)$. Note that in the presence of additional impurity ion species one has $\tau=(T_e/n_e)\Sigma_s n_s Z_s^2/T_s$ where the summation is over all ion species. This expression reduces to $\tau=Z_{\rm eff}(T_e/T_i)$ if the temperatures of all ion species are comparable (which is usually the case). Therefore $Z_i$ (or $Z_{\rm eff}$) and $T_e/T_i$ enter our standard one-species, adiabatic ion runs only as the combination $\tau$, and $R/L_{T_i}$ is irrelevant. Below, we will find that linear nonadiabatic ion effects on ETG modes are indeed negligible. Our nominal core parameters are given by $q=1.4$, $\hat{s}=0.8$, $R/L_n=2.2$, $\tau=1$, $\beta=\alpha=\nu_{ei}=0$; our nominal edge parameters are the same except $R/L_n=10$, $\hat{s}=1$, and $q=2$. Unless otherwise noted, we use either of these parameter sets below.

The method used to derive critical gradients for any given set of parameters is as follows. We generally choose $k_x=0$ (i.e., the ballooning parameter $\theta_0=0$) and a set of $k_y$'s (poloidal wave numbers) in the region of the fastest growing linear ETG modes [for nominal parameters, $(k_y\rho_e)^{\max}\sim 0.3$]. Then we vary $R/L_{T_e}$ and find the linear growth rates as a function of $R/L_{T_e}$ for each value of $k_y$. Linear extrapolation and subsequent minimization over all $k_y$'s yields the final result, $(R/L_{T_e})_{\rm crit}$. This procedure was followed for more than 100 points in parameter space (listed in Appendix A), mostly varying individual parameters around the base case values. The numerical parameters (particularly the time step, the box size and the number of grid points in the parallel direction) were checked regularly to ensure numerical convergence. The influence of modes with a finite value for the ballooning parameter $\theta_0$ has been documented in Appendix B. It is found to be fairly weak for parameters close to the base case.

### A. $\tau$ variation

In the electrostatic and adiabatic limit, the linear dynamics of ETG modes bear strong resemblance to those of ion temperature gradient (ITG) modes, with the roles of electrons and ions reversed. Therefore one expects increasing $\tau$ to have a stabilizing effect on ETG modes since $T_e/T_i$ has a destabilizing effect on ITG modes.[8,9] As is shown in Fig. 1,

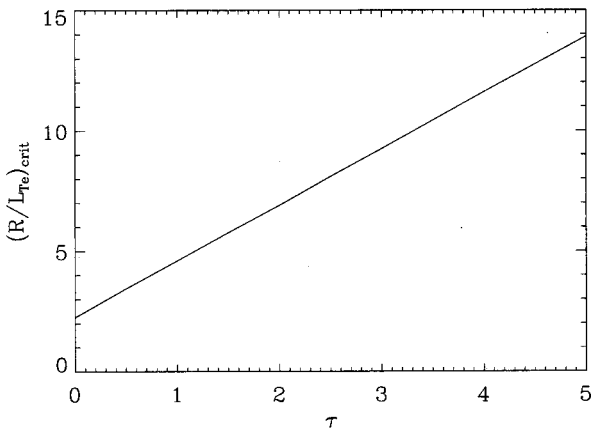


FIG. 1. Dependence of the threshold value $(R/L_{T_e})_{\rm crit}$, on $\tau=Z_{\rm eff}(T_e/T_i)$, for the nominal core parameters.

$(R/L_{T_e})_{\rm crit}$ depends strongly on $\tau$ and can be characterized very well by a linear function, $(R/L_{T_e})_{\rm crit}=2.25+2.33\tau$. Using $\hat{s}=0.4$ instead of the nominal value of $\hat{s}=0.8$ leads to a similar result, $(R/L_{T_e})_{\rm crit}=1.92+2.00\tau$. Since many discharges used for studying $T_e$ profile stiffness involve dominant electron heating which lead to $\tau\gg 1$ in the core plasma, this result is crucial to a correct interpretation of experimental data. It basically tells us that we need to know the $T_i$ and $Z_{\rm eff}$ profiles in addition to the $T_e$ profile in order to make statements about the role of ETG modes in a particular discharge. It is clear that if there are large error bars in $T_i$ and $Z_{\rm eff}$, then it is impossible to calculate $(R/L_{T_e})_{\rm crit}$ with precision.

### B. Magnetic shear variation

A second important quantity is the magnetic shear parameter, $\hat{s}\equiv(r/q)(dq/dr)$. It is known that magnetic shear has a stabilizing effect on many microinstabilities, including ITG and ETG modes.[11] Therefore increasing magnetic shear is expected to lead to a larger value of $(R/L_{T_e})_{\rm crit}$. This trend is clearly observed in Fig. 2, where $\hat{s}$ has been varied between 0.2 and 3. Note that for small values of $\hat{s}$, the mode

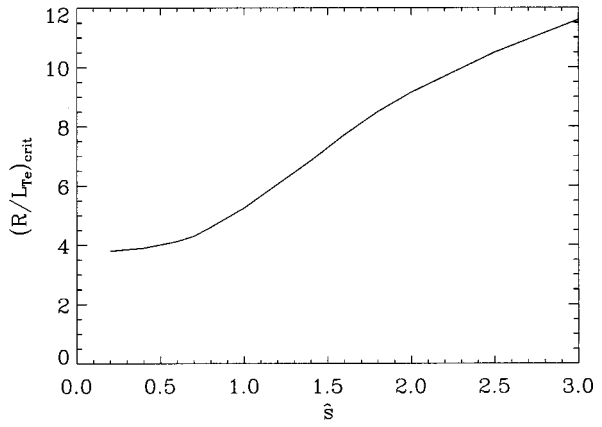


FIG. 2. Dependence of the linear threshold $(R/L_{T_e})_{\rm crit}$, on magnetic shear, $\hat{s}$, for the nominal core parameters.

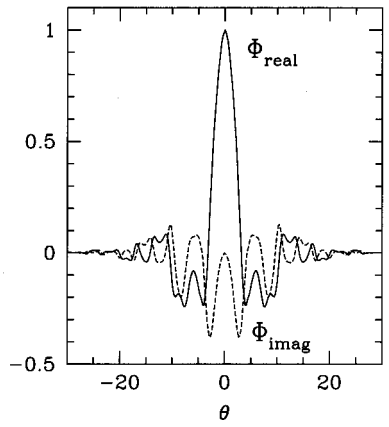


FIG. 3. Electrostatic potential, $\Phi$, as a function of the poloidal angle, $\theta$, for the nominal core parameters except $\hat{s}=0.2$.

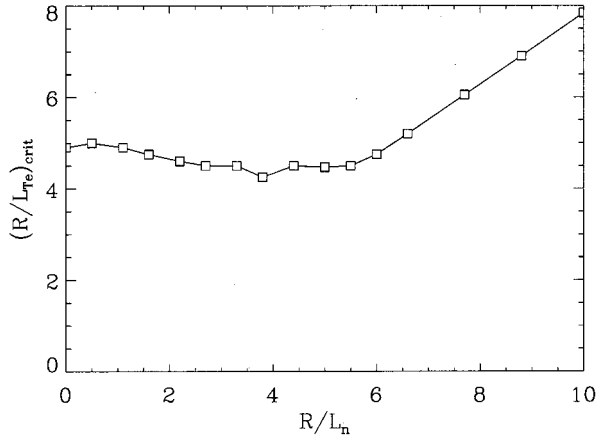


FIG. 5. Dependence of the linear threshold $(R/L_{T_e})_{\mathrm{crit}}$, on the normalized density gradient, $R/L_n$, for the nominal core parameters.

structure becomes very extended along the magnetic field lines as can be seen in Fig. 3. As is shown in Ref. 3, the linear threshold is not relevant for negative shear since the streamer onset condition and the linear threshold $(R/L_{T_e})_{\mathrm{crit}}$ do not coincide; hence we do not consider weak or negative magnetic shear here.

### C. $q$ variation

Very closely related to $\hat{s}$ is the safety factor (inverse rotational transform) $q$. In a simple sheared slab model, the two quantities enter only in the combination $\hat{s}/q=R/L_s$, where $L_s$ is the magnetic shear length. Some of this slab physics is expected and observed to carry over to the toroidal system. Since above we have obtained a fairly strong $\hat{s}$ dependence, we expect a similar finding for $(R/L_{T_e})_{\mathrm{crit}}$ as a function of $q$. The result is plotted in Fig. 4. Note that for $q\to\infty$, i.e., in the local limit, the critical gradient approaches a finite value. The eigenmodes are then characterized by a very pronounced ballooning structure which justifies the local approximation. For $q\gtrsim 2$, $(R/L_{T_e})_{\mathrm{crit}}$ is hardly affected by changes in $q$; for $q\lesssim 2$, it increases strongly with decreasing $q$. This behavior is roughly consistent with $(R/L_{T_e})_{\mathrm{crit}}$ depending primarily on the combination $\hat{s}/q$ (Refs. 10 and 11) although we find that toroidal effects (discussed in Sec. III B) can give a stronger dependence on $q$ at low $\hat{s}$ than this indicates.

### D. $R/L_n$ variation

Many analytic formulas for $(R/L_{T_e})_{\mathrm{crit}}$ in the literature focus on $R/L_n$ dependence and get expressions of the form[8,12–16] $(R/L_{T_e})_{\mathrm{crit}}=\max[\mathcal{A}',\mathcal{B}'(R/L_n)]$ where $2.5\lesssim\mathcal{A}'\lesssim 5$ and $2/3\lesssim\eta_e^{\mathrm{crit}}=\mathcal{B}'\lesssim 1$. Our linear gyrokinetic results are depicted in Fig. 5. They can be well described by this general formula if one sets $\mathcal{A}'=4.5$ and $\eta_e^{\mathrm{crit}}=0.8$. Note that the nominal value, $R/L_n=2.2$, lies well within the flat density profile region of Fig. 5 in which the variation of the critical gradient is fairly small. Therefore all the parameter dependencies of $(R/L_{T_e})_{\mathrm{crit}}$ found above correspond to variations of $\mathcal{A}'$. In order to examine the sensitivity of $\eta_e^{\mathrm{crit}}$ with respect to the other parameters, we choose an ''edge'' reference point which is characterized by our standard parameters except $R/L_n=10$, $\hat{s}=1$, and $q=2$. The results for the variations of $\tau$, $\hat{s}$, and $q$ are displayed in Figs. 6, 7, and 8, respectively. Note that for a wide range of parameters, $\eta_e^{\mathrm{crit}}$ indeed falls

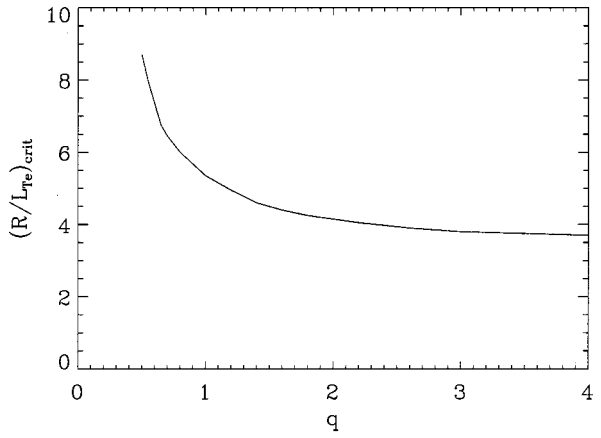


FIG. 4. Dependence of the linear threshold $(R/L_{T_e})_{\mathrm{crit}}$, on the safety factor, $q$, for the nominal core parameters.

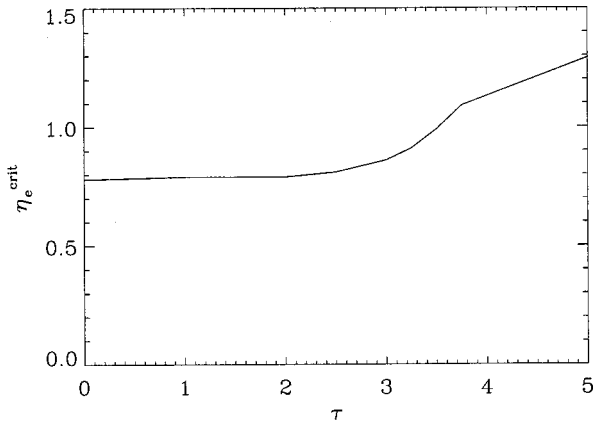


FIG. 6. Dependence of the linear threshold, $\eta_e^{\mathrm{crit}}$, on $\tau=Z_{\mathrm{eff}}(T_e/T_i)$, for the nominal edge parameters.

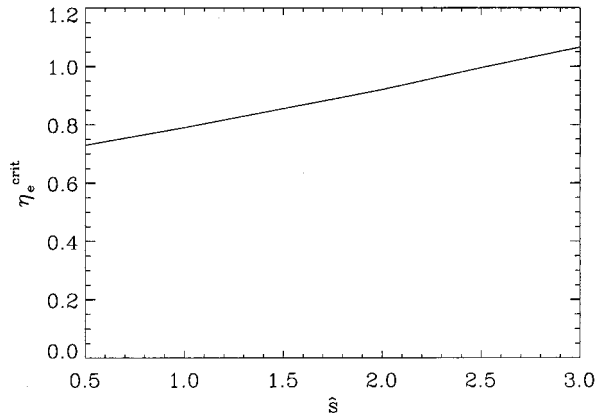


FIG. 7. Dependence of the linear threshold, $\eta_e^{\text{crit}}$, on magnetic shear, $\hat{s}$, for the nominal edge parameters.

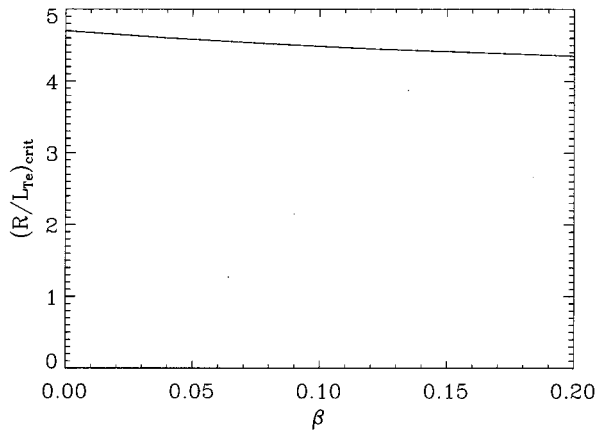


FIG. 9. Dependence of the linear threshold $(R/L_{T_e})_{\text{crit}}$, on the normalized (total) plasma pressure, $\beta$, for the nominal core parameters.

into the range $2/3 \lesssim \eta_e^{\text{crit}} \lesssim 1$ as suggested by the analytical expressions referred to above. In particular, in the high $q$ limit, $\eta_e^{\text{crit}} \to 2/3$.

### E. Finite $\beta$ effects

In the low $\beta$ limit, there are two linear finite $\beta$ effects which can affect the critical gradient for ETG modes, namely magnetic field line fluctuations (finite $\beta$ effects on the dynamics) and Shafranov shift (finite $\beta$ effects on the equilibrium). The influence of these two effects is shown in Figs. 9 and 10. Whereas magnetic field line fluctuations are slightly destabilizing, finite $\alpha = -q^2 R\, d\beta/dr$ has more of an impact on $(R/L_{T_e})_{\text{crit}}$. However, for typical core plasmas with $\alpha \ll 1$, Shafranov shift corrections to the critical gradient generally can be ignored. Moreover, taking finite $\alpha$ effects into account would introduce rather complicated interdependencies with other geometric parameters (like $\hat{s}$) which are hard to capture in a simple algebraic expression.

### F. Nonadiabatic ion effects

All the above simulations used the adiabatic ion approximation which corresponds to the limit $m_i/m_e \to \infty$ (for $\tau \sim 1$). To explore the influence of nonadiabatic ion effects, we performed two-species simulations and varied the ion to electron mass ratio between 100 and 10 000 for both $R/L_{T_i} = 0$ and $R/L_{T_i} = 5$ (see, respectively, the solid and dashed lines in Fig. 11). For realistic mass ratios ($m_i/m_e \gtrsim 2000$) we observe no ion mass dependence, and the impact of $R/L_{T_i}$ on $(R/L_{T_e})_{\text{crit}}$ is negligible.

### G. Collisionality effects

The influence of collisions on the linear threshold is shown in Fig. 12. Here, the normalized electron–ion collision frequency is given by

$$\nu_{ei} R/v_{te} = (6.9 \times 10^{-5}) \lambda R_m n_{e19} T_{e,\text{keV}}^{-2}, \tag{1}$$

where $\lambda$ is the Coulomb parameter. The major radius $R$, the electron density $n_e$, and the electron temperature $T_e$ are given in units of m, $10^{19}\,\text{m}^{-3}$, and keV, respectively. For typical tokamak core parameters, $\lambda \sim 15$, $R_m \sim 1$, $n_{e19} \lesssim 10$, $T_{e,\text{keV}} \gtrsim 1$, we have $\nu_{ei} R/v_{te} \lesssim 0.01$, i.e., there is practically no collisional correction to the linear threshold $(R/L_{T_e})_{\text{crit}}$. This result is, of course, not surprising, given the extremely

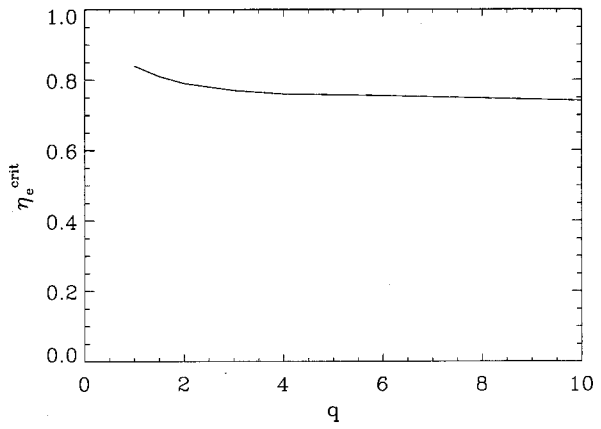


FIG. 8. Dependence of the linear threshold, $\eta_e^{\text{crit}}$, on the safety factor, $q$, for the nominal edge parameters.

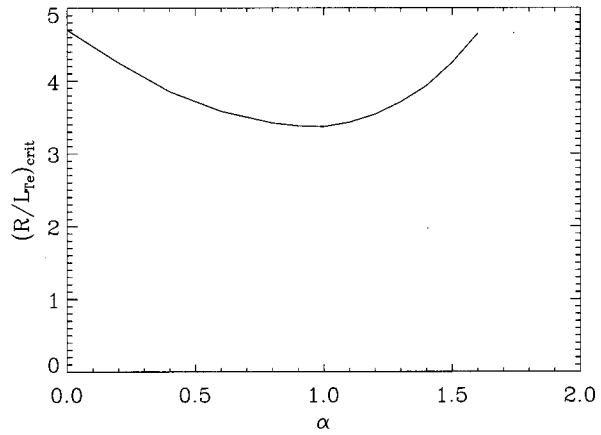


FIG. 10. Dependence of the linear threshold $(R/L_{T_e})_{\text{crit}}$, on the normalized (total) plasma pressure gradient, $\alpha$, for the nominal core parameters.

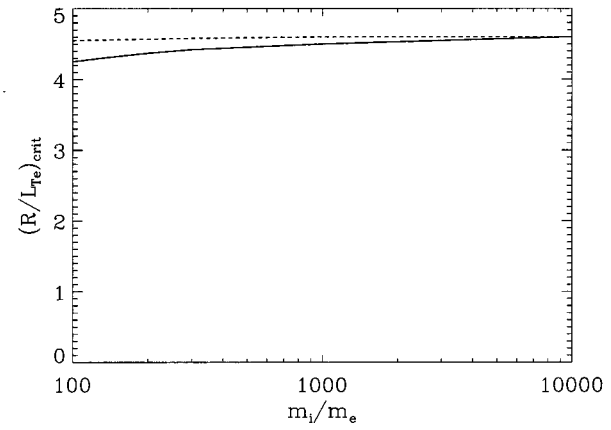


FIG. 11. Dependence of the linear threshold $(R/L_{T_e})_{\mathrm{crit}}$, on the ion to electron mass ratio, $m_i/m_e$, for the nominal core parameters; $R/L_{T_i}=0$ (solid line) and $R/L_{T_i}=5$ (dashed line).

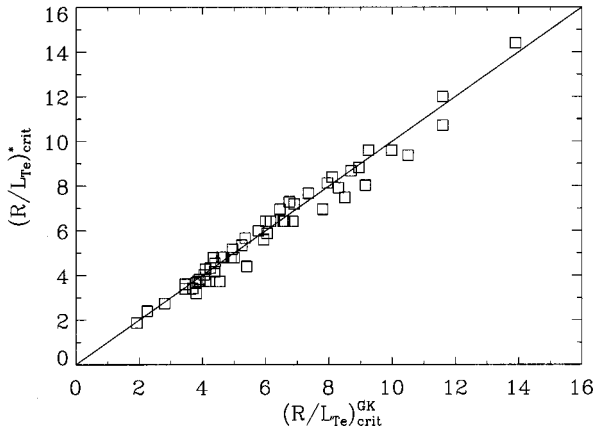


FIG. 13. Linear thresholds $(R/L_{T_e})^{*}_{\mathrm{crit}}$, according to Eq. (4) as a function of the linear thresholds $(R/L_{T_e})^{\mathrm{GK}}_{\mathrm{crit}}$, obtained from linear gyrokinetic simulations.

fast electron dynamics. We also checked the impact of electron–ion collisions on ETG modes for typical edge parameters which was found to be small despite the somewhat larger values of $\nu_{ei}R/v_{te}$.

## III. CRITICAL GRADIENT FORMULA

### A. Circular flux surfaces and large aspect ratio

Before condensing the above results into a compact formula, we consider them in relation to previous analytical results. Like the ITG mode, the ETG mode exists both in a toroidal and in a slab-like version. The toroidal ETG mode is destabilized by the electron ($\nabla B$ and curvature) drift resonance and is subject to a critical value of $R/L_{T_e}$, whereas the slab-like ETG mode is driven by the electron transit resonance and is subject to a critical $L_s/L_{T_e}$ where $L_s$ is the shear length. (Both statements are only valid in the flat density profile limit; otherwise there exists a critical $\eta_e=L_n/L_{T_e}$.) The transition region between two regimes is thus characterized by $R/L_s\sim 1$ or $\hat{s}/q\sim 1$ and the toroidal and slab limits correspond to $\hat{s}/q\ll 1$ and $\hat{s}/q\gg 1$, respectively. Note that for $k_\parallel qR/\hat{s}\sim 1$ and $k_\perp\rho_e\sim 1$, $\hat{s}/q\sim k_\parallel v_{te}/\omega_{De}$ is an estimate of the ratio between the electron transit frequency and the electron drift frequency. In the low and high $\hat{s}/q$ limits, previous analytical results by Romanelli[8] as well as by Hahm and Tang[10] read, respectively,

$$(R/L_{T_e})_{\mathrm{crit}}=\mathcal{A}(1+\tau),\quad \mathcal{A}=4/3 \tag{2}$$

and

$$(L_s/L_{T_e})_{\mathrm{crit}}=\mathcal{B}(1+\tau),\quad \mathcal{B}=3/2(\pi/2)^{1/2}\approx 1.88, \tag{3}$$

where the appropriate change from $T_i/T_e$ (in the original ITG formulas) to $\tau=Z_{\mathrm{eff}}T_e/T_i$ has been made. Romanelli focussed on the electron drift resonance and used the "constant energy resonance" (CER) approximation,[12] $v_\perp^2+2v_\parallel^2\rightarrow 4/3(v_\perp^2+v_\parallel^2)$, whereas Hahm neglected it altogether and focussed on the electron transit resonance instead. Other analytical approaches[13,14] obtained slightly larger values for $\mathcal{A}$ ($\mathcal{A}\sim 1.45$ instead of $\mathcal{A}=4/3$) and did not include the $\tau$ dependence. In the $\nabla B$ approximation,[12] $v_\perp^2+2v_\parallel^2\rightarrow 2v_\perp^2$, one gets $\mathcal{A}=2$; fluid simulations[15] yield $\mathcal{A}=1.7-2.5$. Our linear gyrokinetic simulations agree very well with the Romanelli–CER result in the high $q$ limit; i.e., we find $\mathcal{A}=1.34$ for our standard parameters with $q=200$ instead of $q=1.4$. From a database of more than 100 linear gyrokinetic simulation results for $(R/L_{T_e})_{\mathrm{crit}}$ (see Appendix A), a least-squares fit for the linear threshold of toroidal ETG modes is

$$(R/L_{T_e})_{\mathrm{crit}}=\max\{(1+\tau)(\mathcal{A}+\mathcal{B}\hat{s}/q),\mathcal{C}R/L_n\},$$
$$\mathcal{A}\approx 1.33,\quad \mathcal{B}\approx 1.91,\quad \mathcal{C}\approx 0.8, \tag{4}$$

which in the flat density profile limit is a linear combination of the Romanelli and Hahm–Tang formulas. This formula fits database points with an error bar of $3\sigma=20\%$ (see Fig. 13). It has been derived for $0\leqslant\tau\leqslant 5$, $0.2\leqslant\hat{s}\leqslant 3$, $0.5\leqslant q$, $0\leqslant\hat{s}/q\lesssim 2$, $\alpha\lesssim 0.1$, and arbitrary $R/L_n$, and is naturally expected to work best near the nominal values, $\tau=1$, $\hat{s}=0.8$, $q=1.4$, and $\alpha=0$. Note that $(R/L_{T_e})_{\mathrm{crit}}$ does not depend on $\beta$, $\alpha$, $m_i/m_e$, $R/L_{T_i}$, or $\nu_{ei}$.

However, one caution is that Fig. 13 primarily represents variations of one parameter at a time around two base cases (representing the core or edge). A few multiple parameter

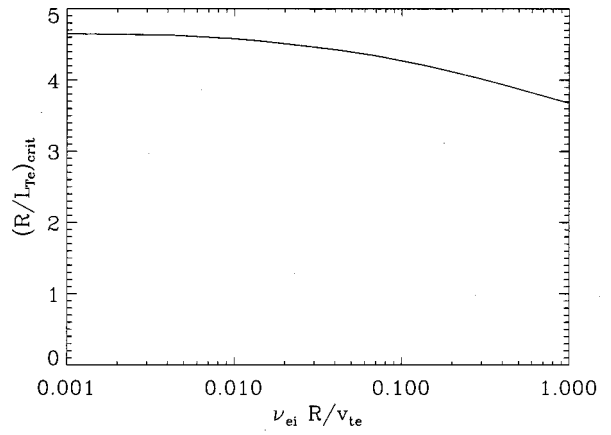


FIG. 12. Dependence of the linear threshold $(R/L_{T_e})_{\mathrm{crit}}$, on the normalized electron–ion collision frequency, $\nu_{ei}R/v_{te}$, for the nominal core parameters.

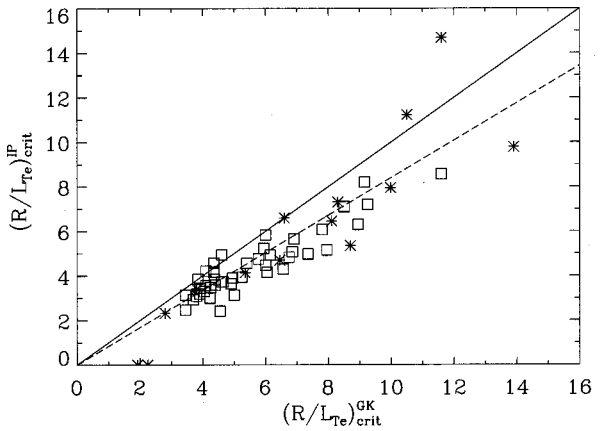


FIG. 14. Linear thresholds $(R/L_{T_e})^{\mathrm{IP}}_{\mathrm{crit}}$, according to the ETG version of the IFS–PPPL critical gradient formula (Ref. 17) as a function of the linear thresholds $(R/L_{T_e})^{\mathrm{GK}}_{\mathrm{crit}}$, obtained from linear gyrokinetic simulations. Stars symbolize data points outside the range of validity of the IFS–PPPL formula. The dashed line represents the finite $\epsilon = r/R_0$ correction (see text and Appendix C).

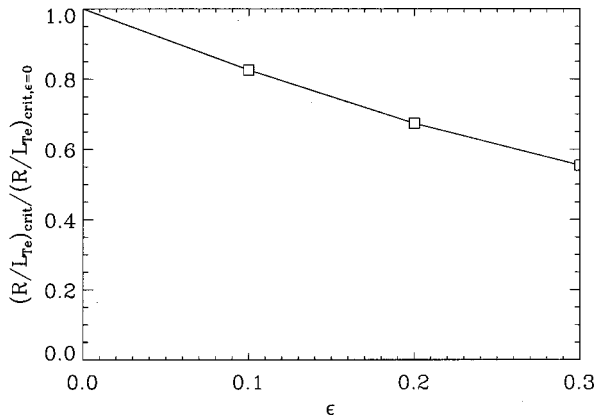


FIG. 15. Dependence of the linear threshold $(R/L_{T_e})_{\mathrm{crit}}$, on the normalized minor radius, $\epsilon = r/R_0$, for the nominal core parameters.

scans have been done, but not extensively, and there are some corners of parameter space where the gyrokinetic critical gradient may deviate more strongly from the simple formulas given here. In particular, one might expect there to be some stabilization at low $q$ even at low magnetic shear (since lowering $q$ corresponds to reducing the connection length between the bad and good curvature regions), which is not adequately represented by this formula which depends on $q$ only through the combination $\hat{s}/q$. For example, at $\hat{s}=0.2$, $q=0.9$, $R/L_n=2.2$, and $\tau=1$, the gyrokinetic code finds $(R/L_{T_e})_{\mathrm{crit}}=4.4$, about 25% above the value of 3.5 given by Eq. (4). This difference is amplified by finite aspect ratio: at $\epsilon=r/R_0=1/6$, $\hat{s}=0.2$, $q=0.9$, $R/L_n=2.2$, and $\tau=1$, the gyrokinetic code gives $(R/L_{T_e})_{\mathrm{crit}}$, about 50% above the value of 2.6 predicted by Eq. (6) below. This low shear, low $q$ regime may be important in the core region of some tokamaks, but it would require more work to fully parameterize this complicated interaction between the $q$, $\hat{s}$ and aspect ratio dependencies.

Despite that, Eq. (4) turns out to be better, simpler, and more general than an ETG version of the original Institute for Fusion Studies–Princeton Plasma Physics Laboratory (IFS–PPPL) critical gradient formula.[17] We modified the IFS–PPPL ITG formula by considering the $Z_{\mathrm{eff}}=1$ limit, redefining $\tau$, and exchanging the roles of $R/L_{T_e}$ and $R/L_{T_i}$. (It is not easy to modify the later version of the IFS–PPPL model,[18] because that model attempted to take fuller account of trapped electron and impurity ion effects, which have no counterpart in the ETG system.) The solid line in Fig. 14 represents a direct comparison of the modified formula with our database. Since the range of validity of the IFS–PPPL formula is restricted to $0.5\leqslant\tau\leqslant4$, $0.5\leqslant\hat{s}\leqslant2$, $0.7\leqslant q\leqslant8$, $0\leqslant R/L_n\leqslant6$, some of our datapoints lie outside this region and are symbolized by stars instead of squares. Even this restricted comparison is inappropriate, however, since the runs in our database were carried out in the large aspect ratio limit, while the IFS–PPPL formulas are based on runs that were carried out in a more realistic local equilibrium model, with a range of $0.1<\epsilon<0.3$. (See Sec. III B and Appendix C for more discussion of this issue.) For the present cases, this difference results in an average 16% reduction in the predicted threshold, shown by the dashed line in Fig. 14. One should compare the fit of the data indicated by open squares to this dashed line with the fit in Fig. 13. The new formula fits a wider region of parameter space with 50% less scatter.

### B. Noncircular flux surfaces and finite aspect ratio

Since the above results were based on a $\hat{s}-\alpha$ model equilibrium which assumes circular flux surfaces and a very large aspect ratio, the applicability of Eq. (4) to experiment is fairly limited. Most present-day and future tokamaks have shaped equilibria and an aspect ratio of 3 or less. Therefore we performed additional linear gyrokinetic simulations employing a local representation of shaped tokamak equilibria[19] in order to generalize Eq. (4). Here, the flux surface shape is specified by elongation, $\kappa$, and triangularity, $\delta$, via

$$R(\theta)/R_0 = 1+\epsilon\cos(\theta+\delta\sin\theta), \quad Z(\theta)/R_0 = \kappa\epsilon\sin\theta, \tag{5}$$

where $R_0$ is the major radius of the flux surface and $\epsilon = r/R_0$. We verified that for $\epsilon\to0$ the $\hat{s}-\alpha$ model results are recovered. With increasing $\epsilon$ we observe a substantial decrease of $(R/L_{T_e})_{\mathrm{crit}}$ as can be seen in Fig. 15. For parameters different than our nominal core parameters (e.g., choosing $\hat{s}=0.4$ or $\hat{s}=1.2$ instead of $\hat{s}=0.8$), we get the same answer within a few percent. Therefore we introduce a finite $\epsilon$ correction factor for $0\leqslant\epsilon\leqslant0.3$,

$$(R/L_{T_e})_{\mathrm{crit}} = \max\{(1+\tau)(1.33+1.91\hat{s}/q) \times(1-1.5\epsilon), 0.8R/L_n\}, \tag{6}$$

which shows that finite aspect ratio effects can be quite important. They can be understood qualitatively in the following way. For toroidal ETG modes with a pronounced ballooning mode structure, what primarily matters is the local value of the major radius at the outboard midplane, $R_{\mathrm{loc}}$. Since $R_{\mathrm{loc}}=R(\theta=0)=(1+\epsilon)R_0$, we therefore have $(R/L_{T_e})_{\mathrm{crit}}\equiv(R_0/L_{T_e})_{\mathrm{crit}}\approx(1-\epsilon)(R_{\mathrm{loc}}/L_{T_e})_{\mathrm{crit}}$

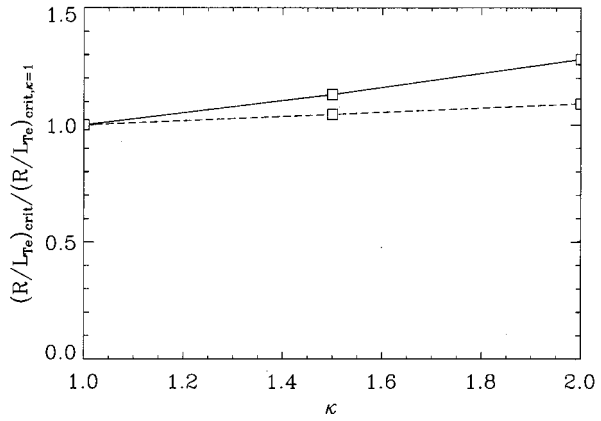


FIG. 16. Dependence of the linear threshold $(R/L_{T_e})_{\mathrm{crit}}$, on the elongation, $\kappa$, for the nominal core parameters except $\epsilon=1/6$. The solid (dashed) line represents a variation of both $\kappa$ and $d\kappa/d\epsilon=(\kappa-1)/\epsilon$ (only $\kappa$).

$\approx(1-\epsilon)(R/L_{T_e})_{\mathrm{crit},\epsilon=0}$, in rough agreement with Eq. (6). Such a finite aspect ratio correction was also included in the IFS–PPPL models.[17,18] Its importance was confirmed by Redd *et al.*[20]

Finally, we set $\epsilon=1/6$ and vary elongation, $\kappa$, and triangularity, $\delta$. The results are shown in Figs. 16 and 17, respectively. Whereas $\delta$ (and its radial variation) has a negligible effect on the linear threshold, the impact of $\kappa$ (and its radial variation) is moderate and can be cast into the form $[1+0.3\epsilon(d\kappa/d\epsilon)]$. Note that the $\kappa$ effect is mainly due to its radial variation $d\kappa/d\epsilon$ which we took to be equal to $(\kappa-1)/\epsilon$ (assuming a linear dependence of $\kappa$ on $\epsilon$). The *direct* impact of $\kappa$ is rather weak. We also did some scans varying the Shafranov shift gradient $\partial R_0/\partial r$ over the modest range of 0 to $-0.3$, but found only a relatively weak 10% variation in $(R/L_{T_e})_{\mathrm{crit}}$, and so we have neglected it in our formulas.

## IV. CONCLUSIONS

Based on comprehensive linear toroidal gyrokinetic simulations, we have derived the following formula for the linear threshold of toroidal ETG modes:

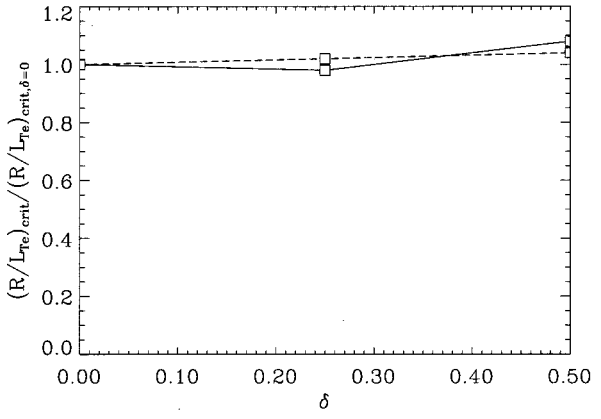


FIG. 17. Dependence of the linear threshold $(R/L_{T_e})_{\mathrm{crit}}$, on the triangularity, $\delta$, for the nominal core parameters except $\epsilon=1/6$. The solid (dashed) line represents a variation of both $\delta$ and $d\delta/d\epsilon=\delta/\epsilon$ (only $\delta$).

$$(R/L_{T_e})_{\mathrm{crit}}=\max\{(1+\tau)(1.33+1.91\hat{s}/q)(1-1.5\epsilon)\times[1+0.3\epsilon(d\kappa/d\epsilon)],0.8R/L_n\}. \quad (7)$$

This expression is an improvement over the ETG version of the IFS–PPPL critical gradient formula and reduces to previous analytical results by Romanelli[8] and by Hahm and Tang[10] in the appropriate limits. It is expected to be applicable to standard tokamak core plasmas, provided $\hat{s}\gtrsim 0.2$ and $\alpha\lesssim 0.1$. Note, however, that finite aspect ratio effects and strong plasma shaping may lead to larger deviations of the gyrokinetic results from Eq. (7) than those shown in Fig. 13 for the large aspect ratio, circular flux surface limit.

It is important to keep in mind that one does not expect advanced tokamak discharges (due to very weak or negative magnetic shear) and tokamak edge plasmas (due to steep profile gradients) to reflect the linear threshold of ETG modes.[3] In these cases, the streamer onset condition and the linear instability threshold do not coincide and the system may deviate substantially from marginality. Therefore we have not attempted to extend Eq. (7) into the negative magnetic shear region.

The ETG threshold is highly sensitive to $\tau=Z_{\mathrm{eff}}T_e/T_i$. Therefore, to investigate electron heat transport by ETG modes, it is crucial to know not only the $T_e$ profile, but also the $T_i$ and $Z_{\mathrm{eff}}$ profiles. The other important quantities (characterizing the magnetic field geometry) are $\hat{s}/q$, $\epsilon$, and $d\kappa/d\epsilon$. The remaining plasma parameters have less impact on the ETG critical gradient.

Turbulence associated with trapped electron modes is likely also to be important in experiments, both for electron thermal and particle transport, as has been shown.[21] We have not addressed the threshold conditions for these modes here.

In the large aspect ratio and low beta limit, Eq. (7) for ETG modes can also be applied to ITG modes with an appropriate redefinition of $\tau$. For $T_e\sim T_i$ and $Z_{\mathrm{eff}}\sim 1$ (which is the standard scenario for a tokamak reactor) one finds $(R/L_{T_i})_{\mathrm{crit}}\sim(R/L_{T_e})_{\mathrm{crit}}$; i.e., ITG and ETG critical gradients almost coincide. In addition, it is often hard in this case to separate the electron and ion channels in the power balance analysis. This suggests that experiments with dominant electron heating (like the ones described in Ref. 22) are particularly valuable in further testing the theoretical idea of $T_e$ profile stiffness caused by ETG modes and TEMs. The critical gradient formula for ETG modes derived here may be a useful tool in this context.

## APPENDIX A: SIMULATION PARAMETERS

Most of the simulation parameters that were used for this study are listed here, indexed by the figure in which they first appear. For each set of parameters, we used 3–7 values of $k_y$ to find the growth rate spectrum, and evaluated this spectrum for 3–5 values of $R/L_{T_e}$. For Figs. 1–2, 4–5, and 9–12, the nominal core parameters were used, with the exception of the variations listed below. For Figs. 6–8, the nominal edge parameters were used, with the exception of the variations listed below. Additional runs were carried out to investigate ancillary issues. There are two curves in Fig. 10, for the two

TABLE I. Simulation parameter variations about the nominal core parameters.

| Fig. | Parameter | Values |
|---|---|---|
| 1 | $\tau$ | 0, 0.5, 1, 1.5,2, 2.5, 3, 4, 5 |
| 2 | $\hat{s}$ | 0.2, 0.4, 0.6, 0.7, 0.8, 1, 1.2, 1.4, 1.6, 1.8, 2, 2.5, 3 |
| 4 | $q$ | 0.5, 0.55, 0.6, 0.65, 0.7, 0.8, 1, 1.2, 1.4, 1.6, 1.8, 2.2, 2.6, 3, 4 |
| 5 | $R/L_n$ | 0, 0.5, 1.1, 1.6, 2.2, 2.7, 3.3, 3.8, 4.4, 5, 5.5, 6, 6.6, 7.7, 8.8, 10 |
| 6 | $\tau$ | 0, 1, 2, 2.5, 3, 3.25, 3.5, 3.75, 4, 4.5, 5 |
| 7 | $\hat{s}$ | 0.5, 1, 1.5, 2, 2.5, 3 |
| 8 | $q$ | 1, 1.5, 2, 3, 4, 6, 8, 10 |
| 9 | $\beta$ | 0, 0.04, 0.08, 0.12, 0.16, 0.2 |
| 10 | $\alpha$ | 0, 0.2, 0.4, 0.6, 0.8, 0.9, 1, 1.1, 1.2, 1.3, 1.4, 1.5, 1.6 |
| 11(a) | $m_i/m_e$ | 100, 130, 200, 300, 100, 1000 |
| 11(b) | $m_i/m_e$ | 100, 130, 200, 300, 100, 1000 |
| 12 | $\nu_{ei}R/v_{te}$ | 0.001, 0.0042, 0.01, 0.014, 0.028, 0.042, 0.071, 0.14, 0.28, 1 |

different values of $R/L_{T_i}$; these are indicated in Table I by 11(a) and 11(b). Approximately 3000 linear GS2 runs were carried out in all.

## APPENDIX B: MODES WITH FINITE BALLOONING PARAMETER

As stated in Sec. II, the derivation of Eq. (7) is based on the assumption that the fastest growing linear ETG mode for any given $k_y$ is characterized by $\theta_0=0$ ($k_x=0$). Although this is true under most circumstances, there are notable exceptions. We checked the results underlying Eq. (7) when $\theta_0\neq 0$ modes are allowed and found that for both large magnetic shear, $1.2\lesssim\hat{s}\lesssim 2.5$, or large safety factor, $q\gtrsim 3$, one may indeed obtain lower values for $(R/L_{T_e})_{\rm crit}$ (see Figs. 18 and 19). However, despite these changes, the fit formula is still a good approximation for the critical gradient. The results corresponding to the scans in $\tau$ (Fig. 1), $R/L_n$ (Fig. 5), $\beta$ (Fig. 9), and $\alpha$ (Fig. 10) as well as the edge parameter results (Figs. 6–8) are not affected by $\theta_0\neq 0$ modes.

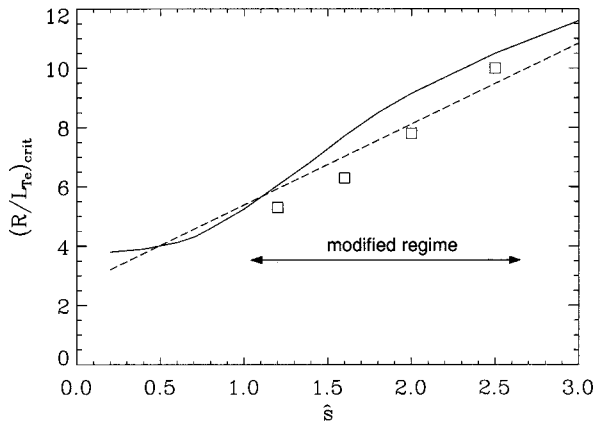


FIG. 18. Dependence of the linear threshold $(R/L_{T_e})_{\rm crit}$, on magnetic shear, $\hat{s}$, for the nominal core parameters. Shown are the gyrokinetic results for modes with $\theta_0=0$ (solid line) and $\theta_0\neq 0$ (squares) as well as the fit formula, Eq. (7) (dashed line).

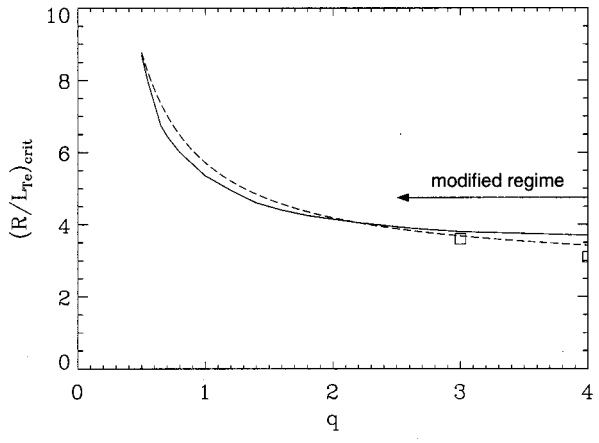


FIG. 19. Dependence of the linear threshold $(R/L_{T_e})_{\rm crit}$, on the safety factor, $q$, for the nominal core parameters. Shown are the gyrokinetic results for modes with $\theta_0=0$ (solid line) and $\theta_0\neq 0$ (squares) as well as the fit formula, Eq. (7) (dashed line).

Increasing both $\hat{s}$ and $q$ at once (from $\hat{s}=0.8$, $q=1.4$ to $\hat{s}=1.5$, $q=2.4$), there is a synergetic effect in that the importance of $\theta_0\neq 0$ modes is enhanced. For $\epsilon=0$, $(R/L_{T_e})_{\rm crit}$ drops from 6.0 (at $k_y=0.35$ and $\theta_0=0$) to 3.6 (at $k_y=0.35$ and $\theta_0=1.2$), whereas the fit formula predicts an intermediate value of 5.1. Fortunately, this discrepancy is reduced at finite $\epsilon$. For example, for $\epsilon=1/6$, $(R/L_{T_e})_{\rm crit}$ drops from 4.4 (at $k_y=0.15$ and $\theta_0=0$) to 3.5 (at $k_y=0.3$ and $\theta_0=0.6$), with the fit formula predicting 3.8.

One can come up with a simple picture of why the first modes to go unstable may have $\theta_0\neq 0$. In the fluid theory described in Chap. 1 of Ref. 23, marginal stability occurs at

$$(R/L_{T_e})_{\rm crit}\approx\langle\omega_{*T}/\omega_d\rangle=2\langle[\cos\theta+\hat{s}(\theta-\theta_0)\sin\theta]\rangle,$$

where $\tau=1$ and $(R/L_n, k_\perp\rho_e)\to 0$; $\langle\cdots\rangle$ denotes an averaging process over the mode stucture in $\theta$ space. Let us assume that we are in a parameter regime that allows for strong ballooning. For ETG modes localized at the outer midplane ($\theta\sim\theta_0=0$) one thus gets $(R/L_{T_e})_{\rm crit}\sim 2$, but for ETG modes localized above or below the midplane ($\theta\sim\theta_0\neq 0$), the linear threshold can be lowered. In reality, the ETG modes will always have some finite extent along $\theta$ and average over different values of the right-hand side of the above equation. But for large values of the safety factor, $q$ (i.e., in the local limit) and at intermediate magnetic shear, $1\lesssim\hat{s}\lesssim q$, they can localize more easily (see the discussion in Sec. III A). This may lead to a reduction of $(R/L_{T_e})_{\rm crit}$ as is observed in Figs. 18 and 19.

## APPENDIX C: COMPARISON WITH IFS–PPPL MODEL

The original IFS–PPPL model did not include any points evaluated at $\epsilon=0$. This complicates the comparison of the present database with the modified IFS–PPPL formula. The dashed line in Fig. 13 represents the prediction from the modified IFS–PPPL model, extrapolated back to $\epsilon=0$ as follows.

We define $X \equiv (R/L_{T_e})_{\mathrm{crit}}$, indicate the IFS–PPPL prediction as modified to describe the linear ETG threshold by $X^{\mathrm{IP}}$, and indicate the result from Eq. (6) by $X^*$. With this notation, Eq. (6) may be written

$$X^* = (1 - 1.5\epsilon) X^*_{\epsilon=0}.$$

Similarly, for $\hat{s} \sim 1$, the modified IFS–PPPL formula is approximately

$$X^{\mathrm{IP}} = (1 - 0.85\epsilon) X^{\mathrm{IP}}_{\epsilon=0}.$$

Assuming the formulas agree over the range of $\epsilon$ that was used to generate the IFS–PPPL model is equivalent to asserting that $X^* = X^{\mathrm{IP}}$ holds in this range. Extrapolating backwards from a typical value of $\epsilon = 0.2$, we find

$$X^{\mathrm{IP}}_{\epsilon=0} = 0.84 X^*_{\epsilon=0}.$$

Together with the excellent fit in Fig. 12, this is the origin of the dashed line in Fig. 13. Clearly, it is only approximate.

[1] F. Jenko, W. Dorland, M. Kotschenreuther, and B. N. Rogers, Phys. Plasmas **7**, 1904 (2000).
[2] W. Dorland, F. Jenko, M. Kotschenreuther, and B. N. Rogers, Phys. Rev. Lett. **85**, 5579 (2000).
[3] F. Jenko, W. Dorland, and G. T. Hoang, "Theory of electron temperature profile stiffness," submitted to Phys. Rev. Lett.
[4] M. Kotschenreuther, G. Rewoldt, and W. M. Tang, Comput. Phys. Commun. **88**, 128 (1995).
[5] T. Antonsen and B. Lane, Phys. Fluids **23**, 1205 (1980).
[6] E. A. Frieman and L. Chen, Phys. Fluids **25**, 502 (1982).
[7] J. W. Connor, R. J. Hastie, and J. B. Taylor, Phys. Rev. Lett. **40**, 396 (1978).
[8] F. Romanelli, Phys. Fluids B **1**, 1018 (1989).
[9] X. Q. Xu and M. N. Rosenbluth, Phys. Fluids B **3**, 627 (1991).
[10] T. S. Hahm and W. M. Tang, Phys. Fluids B **1**, 1185 (1989).
[11] J. Q. Dong, W. Horton, and J. Y. Kim, Phys. Fluids B **4**, 1867 (1992).
[12] F. Romanelli and S. Briguglio, Phys. Fluids B **2**, 754 (1990).
[13] H. Biglari, P. H. Diamond, and M. N. Rosenbluth, Phys. Fluids B **1**, 109 (1989).
[14] R. R. Dominguez and M. N. Rosenbluth, Nucl. Fusion **29**, 844 (1989).
[15] R. R. Dominguez and R. E. Waltz, Nucl. Fusion **29**, 885 (1989).
[16] W. Horton, B. G. Hong, and W. M. Tang, Phys. Fluids **31**, 2971 (1988).
[17] W. Dorland, M. Kotschenreuther, M. Beer *et al.*, *Plasma Physics and Controlled Nuclear Fusion Research 1994* (International Atomic Energy Agency, Vienna, 1996), Vol. 3, p. 463.
[18] M. Kotschenreuther, W. Dorland, G. W. Hammett, and M. A. Beer, Phys. Plasmas **2**, 2381 (1995).
[19] R. L. Miller, M. S. Chu, J. M. Greene, Y. R. Lin-Liu, and R. E. Waltz, Phys. Plasmas **5**, 973 (1998).
[20] A. J. Redd, A. H. Kritz, G. Batemann, G. Rewoldt, and W. M. Tang, Phys. Plasmas **6**, 1162 (1999).
[21] G. W. Hammett, M. A. Beer, J. C. Cummings *et al.*, in *Plasma Physics and Controlled Nuclear Fusion Research 1994* (International Atomic Energy Agency, Vienna, 1996), Vol 3, p. 273; M. A. Beer, G. W. Hammett, G. Rewoldt, E. J. Synakowski, M. C. Zarnstorff, and W. Dorland, Phys. Plasmas **4**, 1792 (1997).
[22] F. Ryter, F. Leuterer, G. Pereverzev, H.-U. Fahrbach, J. Stober, W. Suttrop, and ASDEX Upgrade Team, Phys. Rev. Lett. **86**, 2325 (2001).
[23] M. A. Beer, Ph.D. thesis, Princeton University, 1995.